N-terminal autoprocessing and acetylation of MARTX Makes-Caterpillars Floppy-like effector is stimulated by ADP-Ribosylation Factor 1 in advance of Golgi fragmentation

Alfa Herrera[1], John Muroski[2], Ranjan Sengupta[3†], Hong Hanh Nguyen[2‡], Shivangi Agarwal[1§], Rachel R. Ogorzalek Loo[5], Seema Mattoo[3, 4], Joseph A. Loo[2,5], Karla J. F. Satchell[1]

[1]Department of Microbiology-Immunology, Northwestern University Feinberg School of Medicine, Chicago, IL 60611, USA

[2]Department of Chemistry and Biochemistry, University of California-Los Angeles, Los Angeles, CA, 90095, USA

[3]Department of Biological Sciences, and [4]Purdue Institute for Inflammation, Immunology and Infectious Diseases, Purdue University, West Lafayette, IN, 47907, USA

[5]Department of Biological Chemistry, David Geffen School of Medicine, UCLA Molecular Biology Institute, and UCLA/DOE Institute of Genomics and Proteomics, University of California-Los Angeles, Los Angeles, CA, 90095, USA

Current addresses:

[†]Department of Medicinal Chemistry and Molecular Pharmacology, Purdue University, West Lafayette, IN, 47907, USA

[‡]IndoChina Center of Excellence, Transmed Co., Ltd, Ho Chi Minh city, Vietnam

[§]Department of Internal Medicine, Rush University Medical Center, Chicago IL 60612 USA

ABSTRACT

Studies have successfully elucidated the mechanism of action of several effector domains that comprise the MARTX toxins of *Vibrio vulnificus*. However, the biochemical linkage between the cysteine proteolytic activity of Makes Caterpillars Floppy-like (MCF) effector and its cellular effects remains unknown. In this study, we identify the host cell factors that activate *in vivo* and *in vitro* MCF autoprocessing as ADP-Ribosylation Factor 1 (ARF1) and ADP-ribosylation Factor 3 (ARF3). Autoprocessing activity is enhanced when ARF1 is in its active (GTP-bound) form compared to the inactive (GDP-bound) form. Subsequent to auto-cleavage, MCF is acetylated on its exposed N-terminal glycine residue. Acetylation apparently does not dictate subcellular localization, as MCF is found localized throughout the cell. However, the cleaved form of MCF gains the ability to bind to the specialized lipid phosphatidylinositol 5-phosphate enriched in Golgi and other membranes necessary for endocytic trafficking, suggesting a fraction of MCF may be subcellular localized. Traditional thin-section electron microscopy, high-resolution cryoAPEX localization, and fluorescent microscopy show that MCF causes Golgi dispersal resulting in extensive vesiculation. In addition, host mitochondria are disrupted and fragmented. Surprisingly, ARF1 is not itself processed or post-translationally modified by MCF. Further, only catalytically inactive MCF stably associates with ARF1, thus serving as a substrate trap. Our data indicate that ARF1 is a cross-kingdom activator of MCF, but reveal that MCF mediates cytotoxicity likely by directly targeting another yet to be identified protein. This study begins to elucidate the biochemical activity of this important domain and gives insight into how it may promote disease progression.

48 **1. INTRODUCTION**

49 *Vibrio vulnificus* is a Gram-negative pathogen found in warm marine environments that is capable
50 of causing life-threatening gastrointestinal and wound infections, particularly from handling or
51 consumption of seafood. These infections are rare, although the incidence of *V. vulnificus* is
52 increasing in the US, in part due to expanding geographical distribution due to warming seawaters
53 (Baker-Austin et al., 2012; Deeb, Tufford, Scott, Moore, & Dow, 2018; King et al., 2019). The
54 rising incidence of *V. vulnificus* infections is extremely concerning given its severity, as it often
55 leads to fatal sepsis (Horseman & Surani, 2011). About 90% of patients are hospitalized and more
56 than 50% die, often as fast as 48 hours after symptom onset (CDC, 2014; Gulig, Bourdage, &
57 Starks, 2005). These infections are costly due to high mortality rates and negative impact on
58 economies that depend on recreation and seafood harvesting (Hoffman & Batz, 2015; Morgan,
59 2010). Currently in the US, *V. vulnificus* accounts for only 0.001% of infections, but 3% of all food-
60 related deaths (Mead et al., 1999). According to the US Department of Agriculture, *V. vulnificus*
61 exerts the highest per-case economic burden of any food-borne disease and its total burden
62 exceeds *Shigella* and *Escherichia coli* O157:H7 (Hoffman & Batz, 2015).

63 For both wound and intestinal infections, the primary *V. vulnificus* virulence factor
64 associated with sepsis and subsequent death is the composite multifunctional-autoprocessing
65 repeats-in-toxins (MARTX) toxin encoded by the gene *rtxA1* (Satchell, 2015). Expression of the
66 MARTX toxin can increase lethality of *V. vulnificus* up to 2600-fold (Kwak, Jeong, & Satchell,
67 2011). The *V. vulnificus* MARTX toxin is secreted from the bacterium as a single large polypeptide.
68 It is composed of conserved glycine-rich repeats at both the N- and C-termini between which
69 there are variable effector domains and a cysteine protease domain (CPD). The repeat regions
70 are thought to recognize eukaryotic host cells via a yet undetermined mechanism and then form
71 a pore in the plasma membrane. The effectors and CPD are then translocated across the
72 membrane through this pore. Within the cell, the CPD binds inositol hexakisphosphate, which
73 activates the CPD to auto-cleave at multiple sites to release each of the arrayed effectors

74 individually into the host cytoplasm. The MARTX toxin thus serves as an effector delivery platform
75 for translocation of multiple toxic virulence factors inside cells as a single bolus (Gavin & Satchell,
76 2015; Kim, 2018; Satchell, 2015).

77 Across distinct *V. vulnificus* isolates, the effector content can vary from 2 to 5 effectors
78 selected from a total of nine known effector domains (Kwak et al., 2011; Ziolo et al., 2014). The
79 effector repertoire can be exchanged by horizontal gene transfer and recombination events such
80 that even closely related strains can have different MARTX toxin variants (Roig, Gonzalez-
81 Candelas, & Amaro, 2011). The effector domain most commonly present in *V. vulnificus* MARTX
82 toxins is the Makes Caterpillars Floppy-like (MCF) effector domain (Agarwal, Agarwal, Biancucci,
83 & Satchell, 2015; Agarwal, Zhu, Gius, & Satchell, 2015). It is found in all Biotype 1 and 2 strains
84 that cause human infections and is even duplicated in the MARTX toxin of some strains (Kwak et
85 al., 2011; Roig et al., 2011).

86 The MCF effector domain is 376 aa in size. In representative strain CMCP6, MCF is
87 encoded by gene *rtxA1* (*vv2_0479*) nucleotides 9610-10737 to comprise residues 3204-3579 of
88 the full-length MARTX toxin. Once within cells, MCF has been shown to induce the intrinsic
89 apoptotsis pathway, resulting in cell rounding, vesiculation, and loss of cell proliferation (Agarwal,
90 Agarwal, et al., 2015; Agarwal, Zhu, et al., 2015). MCF has been shown to activate caspase-9, 7,
91 3 and PARP-γ, and to induce nuclear shrinkage and fragmentation. It also upregulates the
92 proapoptotic proteins Bax, Bak, and Bad to induce loss of mitochondrial transmembrane potential
93 resulting in increased release of cytochrome c into the cytosol.

94 Sequence homology places MCF into the C58 family of cysteine peptidases (Rawlings,
95 Waller, Barrett, & Bateman, 2014). Site-directed mutagenesis revealed that the conserved Cys-
96 148 residue (aa 3351 in full-length toxin) is essential for MCF cytotoxicity. However, even though
97 other putative catalytic residues His-55 (aa 3258 in full-length toxin) or Asp-142 (aa 3345 in
98 full-length toxin) are conserved by sequence alignment with the C58 peptidases that use a Cys-
99 His-Asp (CHD) catalytic triad, alanine substitution of these residues reduced, but did not eliminate,

100 cell rounding (Agarwal, Agarwal, et al., 2015). Instead, MCF has an Arg-Cys-Asp (RCD) peptide
101 triad at residues 147-149 (aa 3350-3352 in full-length toxin) that is necessary for its cytotoxic
102 effects. A homology search revealed numerous known and putative toxin proteins that contain
103 domains with sequence similarity to MCF that also contain the RCD/Y motif (Agarwal, Agarwal,
104 et al., 2015). We suggest these proteins form a new subfamily of the C58 peptidases. Thus far,
105 no structures of a peptidase from this family has been determined so the structural implications
106 of the RCD/Y motif compared to the CHD motif remain unknown.

107 Upon ectopic expression in host cells, MCF undergoes autoprocessing at its N-terminus
108 cleaving itself between Lys-15 and Gly-16 dependent upon an intact RCD motif (Agarwal,
109 Agarwal, et al., 2015). This autoprocessing could be reproduced with recombinant MCF, but only
110 upon addition of eukaryotic cell lysate to the reaction. In this study, we identify the cross-kingdom
111 autoprocessing-stimulating host factor as Class I and II ADP-ribosylation factors (ARFs), and
112 most prominently ARF1. We further show that subsequent to autoprocessing, the exposed N-
113 terminal Gly-16 is acetylated. MCF then also gains the ability to bind phosphatidylinositol-5-
114 phosphate (PtdInsP5), a lipid enriched on the Golgi apparatus. The expression of MCF in cells
115 then leads to increased vesiculation in the cells caused by dissolution of the Golgi apparatus.
116 Destruction of the Golgi, and also the mitochondria, suggests a mechanism for induction of
117 caspases leading to MARTX toxin dependent cellular apoptosis (Lee, Choi, & Kim, 2008).
118

119 **2. RESULTS**

120 **2.1. Purified ARF1 and ARF3 GTPases induce autoprocessing of recombinant MCF protein**

121 MCF is known to be induced to auto-cleave by an unidentified eukaryotic host cell factor. To
122 identify this host factor, MCF encoding gene sequences were truncated to mimic the cleaved form
123 of MCF (cMCF, aa 16-376) and then modified to alter the codon for the catalytic Cys-148 to
124 alanine ($cMCF^{CA}$). The modified gene was ectopically expressed in human embryonic kidney
125 (HEK) 293T cells fused with an N-terminal FLAG and C-terminal hemagglutinin (HA) tag to

126 express dual-tagged cMCF^{CA} (dt-cMCF^{CA}). Anti-HA immunoprecipitation revealed a protein of
127 approximately 20 kDa that bound to dt-cMCF^{CA} (Fig 1A). Peptide sequencing of the excised band
128 revealed nine unique peptides. Seven mapped to the human protein ADP-Ribosylation Factor
129 (ARF1) and the nearly identical protein ADP-Ribosylation Factor 3 (ARF3). One peptide matched
130 exclusively to ADP-Ribosylation Factor (ARF4) and another to ADP-Ribosylation Factor 6 (ARF6)
131 (Fig 1B).

132 To confirm identification of ARF1 as a host factor that induces autoprocessing, full-length
133 MCF (flMCF) with and without its catalytic Cys-148 (flMCF^{CA}), cleaved MCF (cMCF), and
134 catalytically inactive cleaved MCF (cMCF^{CA}) were purified as 6xHis-tagged recombinant proteins.
135 Truncated Δ17ARF1 fused with glutathione-S-transferase (GST-Δ17ARF1) was purified as
136 removal of the flexible N-terminus is known to increase protein solubility (Kahn et al., 1992). Both
137 catalytically active and inactive flMCF and cMCF forms co-precipitated with GST-Δ17ARF1
138 confirming that MCF and ARF1 interact and that the binding does not involve the flexible N-
139 terminus of ARF1 (Fig 1C).

140 The flMCF proteins were next incubated with Δ17ARF1 purified as a 6x-tagged
141 recombinant protein to test stimulation of autoprocessing. Δ17ARF1 stimulated flMCF cleavage
142 and the processing was autocatalytic as flMCF^{CA} was not processed even in the presence of
143 Δ17ARF1 (Fig 1D). Δ17ARF3 and Δ17ARF4 also stimulated autoprocessing, while Δ17ARF6 did
144 not (Fig. 1E). Full-length ARF1 and ARF3 with the N-terminus intact were also able to stimulate
145 autoprocessing with similar kinetics (Fig. 1F).

146 ARFs are all members of the Ras superfamily of small GTPases that cycle between an
147 active (GTP-bound) and inactive (GDP-bound) form. ARF1 pre-loaded with GTP-analog GppNHp
148 induced more rapid and more complete MCF auto-cleavage (85 +/- 3%) compared to ARF1 pre-
149 loaded with GDP (29 +/- 13%) (Fig 1G).

150 Altogether, these data demonstrate that ARF1 is a host factor that binds and stimulates
151 autoprocessing of MCF. The nearly identical protein Class I ARF3 and the Class II ARF4 can also
152 serve as cross-kingdom host factors capable of inducing MCF auto-cleavage. Further, there is a
153 strong preference for induction of autoprocessing by the active (GTP-bound) form of ARFs.
154

155 **2.2. MCF^{CA} functions as a trap for ARF1 in cells**

156 To identify which of the major ARF isoforms are important within cells for induced autoprocessing,
157 dt-cMCF^{CA} was co-expressed in HEK293T cells with Myc-tagged ARF proteins. ARF1, but not
158 ARF4 or ARF6, co-immunoprecipitated with cMCF^{CA} (Fig 2A). We were unable to reproducibly
159 pulldown ARF3 with dt-cMCF^{CA} across independent experiments and thus were not able to
160 confirm this interaction. Thus, although multiple ARF isoforms stimulate MCF autoprocessing *in*
161 *vitro*, ARF1 is the only isoform that consistently associates with dt-cMCF^{CA} in cells.

162 Consistent with its function as a host factor for induction of autoprocessing of flMCF, ARF1
163 was also co-immunoprecipitated with dt-flMCF^{CA}, indicating interaction between the two proteins
164 occurs prior to the autoprocessing event. By contrast, ARF1 did not co-immunoprecipitate with
165 either dt-flMCF or dt-cMCF if the catalytic Cys-148 was not modified to alanine (Fig 2B). This is
166 not due to an inability of the proteins to associate because, as shown above, GST-Δ17ARF1 co-
167 precipitated with both catalytically active and inactive flMCF and cMCF *in vitro* (Fig 1C). These
168 data indicate that, in cells, MCF autoprocessing results in release and/or loss of the ability to bind
169 to ARFs such that only catalytically inactive MCF functions as a protein trap. Further, since
170 overexpression or delivery of catalytically inactive MCF to cells does not itself cause cytotoxicity
171 (Agarwal, Agarwal, et al., 2015; Agarwal, Zhu, et al., 2015), trapping of ARFs is not sufficient for
172 MCF-mediated cytotoxicity.

173 Repeated attempts to identify an MCF-specific processing or post-translational
174 modification of ARF1 or ARF3 *in vitro* or on proteins recovered from cells were not successful.
175 We did not observe any visible changes to the size of ARF1-Myc when co-transfected with either

176 full length or cMCF or the catalytically inactive versions by western blot (Fig 2A-B). We also did
177 not identify any MCF-specific post-translational modifications on ARF1 or ARF3 using a
178 bottom-up proteomics strategy (Supplemental Fig 1). Therefore, it is possible that while ARF1 can
179 induce MCF to autoprocess, MCF-mediated processing or covalent modification of ARFs is not
180 the mechanism of cell cytotoxicity. Thus, we speculate the preferred association of MCF with
181 ARF1-GTP functions to localize MCF to a proper membrane where it is activated by
182 autoprocessing, but then released from ARF1, possibly to access other targets.
183
184 **2.3. After autoprocessing, MCF is N-terminally acetylated**
185 In cells, MCF undergoes additional modifications. Previously, attempts to identify the
186 autoprocessing site on MCF from protein recovered from cells revealed the N-terminus was
187 blocked to Edman degradation. The N-terminal block does not occur *in vitro*. The Edman
188 degradation analysis of immunoprecipitated MCF was repeated for this study and confirmed to
189 be blocked (Supplemental Fig 2A and 2B). Further, two-dimensional gel analysis of MCF
190 expressed in cells showed that dt-flMCF undergoes *in vivo* autoprocessing to release its N-
191 terminal FLAG tag, coincident with a shift in electrophoretic mobility, which was detected by
192 western blotting using anti-HA antibody directed against the C-terminal tag. It was further noted
193 that processed flMCF separated into discrete populations that differ in isoelectric point.
194 Catalytically inactive dt-flMCF^{CA} does not shift in size, consistent with the autoprocessing being
195 autocatalytic, or separate into different populations (Fig 3A).
196 To identify potential post-translational modifications on MCF, the four individual
197 populations were excised and analyzed by bottom-up mass proteomics (Fig 3B); the analysis
198 revealed that Gly-16, which is exposed following auto-cleavage, was acetylated (Fig 3C and
199 Supplemental Fig 3). The acetylation was identified in populations 2 and 3, but not population 1
200 or 4 (Supplemental Fig 3). Acetylation of other lysine residues in populations 2, 3, and 4 was also
201 observed, but the modified lysine varied across different experiments or replicates of the same

202 population (Fig 3C and Supplemental Fig 3). These observations indicate that only the acetylation
203 of the N-terminal glycine of MCF is specific, while other acetylation events are stochastic
204 modifications that likely arise from overexpression of a protein with many surface exposed lysine
205 residues.
206
207 **2.4. MCF binds Golgi enriched lipids and causes Golgi dispersion**
208 ARF1 and ARF3 most commonly localize to the Golgi apparatus (Hofmann & Munro, 2006; Tsai,
209 Adamik, Haun, Moss, & Vaughan, 1993) and ARF association with the Golgi is dependent upon
210 its activation by GTP. As MCF preferentially associates with active ARFs, it may facilitate targeting
211 to subcellular organelles. In addition, many proteins are directed to subcellular organelles by
212 binding specific lipids. Lipid overlay assays show cMCF, but not flMCF, preferentially binds
213 PtdIns5P (Fig 4). PtdIns5P is not well described but has a suggested role in membrane trafficking
214 and is enriched in Golgi membranes (Backer, 2010). Thus GTP-bound ARFs may bring MCF to
215 the Golgi for activation, but cMCF might be retained at the Golgi even after dissociation from
216 ARFs due to a gain of function for PtdIns5P binding.
217 The co-localization of MCF with the Golgi was thus assessed by immunofluorescence (IF).
218 In cells transfected to express only green fluorescent protein (eGFP), the human Golgi matrix
219 protein GM130, a marker for the *cis*-Golgi, showed the Golgi apparatus as tight and condensed
220 at its expected position near the nuclei (Fig 5A). Catalytically inactive MCF^{CA} frequently co-
221 localized with GM130, although protein also diffused throughout the cell (Fig 5A).
222 However, the co-localization of MCF^{CA} does not inform about possible localization of MCF
223 after dissociation from ARFs. Thus, we examined if catalytically active MCF retains association
224 with the Golgi or other membranes. While the Golgi in cells expressing flMCF-eGFP was disrupted
225 and dispersed, attempts to co-localize MCF were not conclusive. Indeed, GM130 in these cells
226 was not visible unless the image was overexposed (Fig 5A). Similar dispersion was not observed
227 for the endoplasmic reticulum (ER)-associated protein calreticulin in cells transfected to express

228 MCF-eGFP (Supplemental Fig 4). Thus, catalytically active MCF was found to disrupt the Golgi
229 of host cells and the resulting damage prevented resolution of its intracellular localization using
230 IF.
231
232 **2.5. Golgi dispersion and mitochondrial fragmentation occurs when MCF is delivered to**
233 **cells by the bacterium**
234 To ensure Golgi disruption is not an artifact of overexpression of MCF by transient
235 transfection, cells treated with live *V. vulnificus* were imaged. Sequences corresponding to the
236 MARTX toxin effectors had been previously deleted from the *rtxA1* gene in strain CMCP6 strain
237 and replaced with in-frame beta-lactamase gene sequences to generate a fusion gene *rtxA1::bla*
238 that encodes an effector-less MARTX toxin but delivers beta-lactamase as a marker for intact
239 protein and translocation function. Sequences for MCF were then introduced to generate
240 *rtxA1::mcf-bla* that expresses a MARTX toxin that delivers only the MCF effector (Agarwal, Zhu,
241 et al., 2015).
242 Treatment of cells with CMCP6 *rtxA1::bla* showed the Golgi remained perinuclear and
243 condensed similar to non-intoxicated cells. In contrast, cells intoxicated with CMCP6 *rtxA1::mcf-*
244 *bla* showed Golgi was dispersed and spreading away from the nucleus (Fig 5B). In addition, the
245 impact of MCF on mitochondria was also visualized using MitoTracker Green FM. The
246 mitochondrial network of cells treated with the control strain CMCP6 *rtxA1::bla* appeared as long
247 dynamic fragments throughout the cell (Fig 6). In contrast, the mitochondria of cells intoxicated
248 with CMCP6 *rtxA1::mcf-bla* were shortened and fragmented in comparison. The mitochondrial
249 network in these cells was composed of more short round fragments than long branches (Fig 6).
250 These data show that MCF delivered to cells by bacteria induces intracellular damage of
251 both the Golgi and the mitochondria.
252

253 **2.6. Transmission electron microscopy shows MCF induces extensive vesiculation of the**
254 **Golgi apparatus**

255 To gain an ultrastructural understanding of how catalytically active MCF induces Golgi
256 dispersion, transmission electron microscopy was employed. As expected, at 10 hours after
257 transfection, PBS mock transfected HeLa cells showed a Golgi with typical stacked morphology
258 (Fig 7A, green G). By contrast, in cells ectopically expressing MCF, there are a significant number
259 of vesicles (Fig 7B, purple V) in the cytoplasm localized near the Golgi, with some enmeshed
260 within the Golgi complex (Fig 7B, Supplemental Fig 5A). At higher magnification, it was evident
261 that, although some of the Golgi retained a classical stacked morphology some of the cisternae
262 appeared herniated transitioning into a more vesicular morphology (Fig 7B, Supplemental Fig
263 5A). Additionally, an abundance of autolysosomes was also observed. Some autolysosomes
264 contained vesicles, indicating ongoing clearance off these vesicles (Fig 7E). At 15 hours post
265 transfection, the cytoplasm was inundated with a variety of different sized pleomorphic vesicles
266 (Fig 7D, Supplemental Fig 5B). In these cells the typical stacked structure of the Golgi apparatus,
267 which is seen in mock treated cells, was not observed (Fig 7C).

268 The electron microscopy data correlate with the IF observations showing darkened
269 mitochondria at 10 hours post-transfection with condensed disintegrating cristae in cells
270 ectopically expressing MCF (Fig 7G). This was in contrast to control cells where mitochondria
271 have an oval shape, with visible cristae (Fig 7F). These data show that both the mitochondria and
272 the Golgi are impacted by expression of MCF.

273

274 **2.7. MCF localizes to the Golgi apparatus, the membrane of the vesicular structures and**
275 **the cytosol**

276 As both N-terminal acetylation and binding to PtdIns5P could dictate subcellular
277 localization, we investigated localization of MCF using electron microscopy based high resolution
278 cryoAPEX technology (Sengupta, Poderycki, & Mattoo, 2019). Briefly, MCF was expressed in

279 HeLa cells as a fusion with a soybean ascorbate peroxidase (Apex2). This tag catalyzes a
280 peroxide reaction that converts diaminobenzidine (DAB) into an insoluble osmophilic precipitate.
281 This precipitate could then be preferentially and specifically stained with osmium tetroxide thereby
282 revealing the subcellular localization of MCF at a nanometer-scale resolution, with MCF-Apex2
283 expressing cells easily distinguished from non-expressing cells due to dark staining of the
284 cytoplasm and presence of cytoplasmic vesicles compared to the mock transfected control (Fig
285 8B-C, and 8A). This ubiquitous staining of the cytosol indicates a large pool of MCF is present in
286 cytosol. Interestingly, staining was also detected on the membrane of the Golgi stacks visible in
287 samples from the 10-hour time-point as well as on vesicles at both time points (Fig 8B-C, blue
288 arrows). In comparison, control cells transfected with MCF-Apex2 for 10 hours not treated with
289 H_2O_2 exhibit a relatively clear cytoplasm and lack membrane staining of vesicles (Fig 8D). Cells
290 expressing MCF also had darkened staining at the nuclear membrane compared to control cells,
291 indicating a presence of the effector here as well (Fig 8B-C).
292
293 **3. Discussion**
294 ADP-ribosylation factors (ARFs) were first identified as activators of the ADP-ribosylation
295 activity of the bacterial protein cholera toxin (Gillingham & Munro, 2007). They subsequently have
296 been shown to have important roles as regulators of eukaryotic cell membrane trafficking
297 (Gillingham & Munro, 2007; Muthamilarasan, Mangu, Zandkarimi, Prasad, & Baisakh, 2016).
298 Depending on the isoform, they localize to specific subcellular locations, including the Golgi,
299 plasma membrane, and endosomes. The Golgi apparatus is generally composed of tight
300 perinuclear Golgi stacks and plays a central role in membrane trafficking, wherein it receives,
301 post-translationally modifies and sorts proteins from the ER to their appropriate destinations (Liu
302 & Storrie, 2015; Wei & Seemann, 2010). At the Golgi, ARF1 is recognized by its guanine
303 nucleotide exchange factors (GEF), inducing a conformational change that exposes its N-terminal
304 amphipathic helix so that it binds GTP in place of GDP (Behnia, Panic, Whyte, & Munro, 2004).

305 This change allows ARF1 to bind the membrane where it plays an important role in recruiting coat
306 complex protein I, clathrin adapter proteins AP1 and AP2, and other proteins necessary for proper
307 vesicle budding and trafficking. This membrane binding is reversed by GTPase-activating proteins
308 (GAPs) that catalyze hydrolysis of the GTP resulting in ARF1 release from the membrane. The
309 nearly identical protein ARF3 has similar function, behaving indistinguishably in most studies.
310 Given the importance of ARFs and the Golgi to cellular processes, bacteria often manipulate ARF
311 function and Golgi stability to promote bacterial infection.

312 In this study, we show the pro-form of the *V. vulnificus* MARTX effector MCF is activated
313 by autoprocessing upon binding with Class I ARF1 and ARF3. Although MCF can also be
314 stimulated by ARF4 to autoprocess, these proteins do not associate in cells. Notably, MCF can
315 be stimulated to auto-cleave by either the full-length forms of ARF1 and ARF3 or the more stable
316 Δ17 forms of the proteins. This demonstrates that binding of ARF to MCF does not require the
317 first 17 aa that are essential *in vivo* for membrane association.

318 The protein-protein interaction of MCF with ARF1 was confirmed in cells. ARF1 transitions
319 between a GDP- and GTP-bound state dictating its position on and off of the Golgi (Behnia et al.,
320 2004). As MCF is more rapidly and more fully induced to auto-cleave by ARF1-GTP than by
321 ARF1-GDP, MCF is probably preferentially recruited to the Golgi, where it binds ARF1-GTP.
322 Indeed, a low level of active ARF3-GTP at the Golgi under conditions for these experiments may
323 explain our difficulty confirming MCF binding to ARF3 in cells (Tsai et al., 1993).

324 The cell data also support that once ARFs stimulate autoprocessing, they do not continue
325 to stably associate with MCF, unless the catalytic cysteine is inactivated. This is in contrast to
326 studies using purified proteins that show ARF1 can bind to both catalytically active and inactive
327 MCF. We originally surmised this was evidence that ARF1 was modified in cells by catalytically
328 active MCF and then released, although extensive analysis found no cleavage or post-
329 translational modification of ARF1 or ARF3. We therefore conclude that there is a secondary

330 event that alters the structure of MCF after processing to release ARFs and this exchange may
331 require Cys-148.

332 Catalytically inactive cMCF was by contrast able to function as a protein trap for ARFs.
333 Yet, this protein does not cause obvious cytotoxicity when overexpressed in cells (Agarwal,
334 Agarwal, et al., 2015; Agarwal, Zhu, et al., 2015). These data contradict potential models whereby
335 MCF functions simply to sequester ARF from its normal function. Thus, we surmise there is
336 another protein that may be a target for cleavage by catalytically active cleaved MCF. Attempts
337 to identify this host co-factor protein using catalytically inactive MCF as a substrate trap/bait for
338 the initial immunoprecipitation were unsuccessful. It is possible that this protein may be cleaved
339 or degraded in intoxicated cells and thus was difficult to identify using immunoprecipitation
340 strategies.

341 Subsequent to autoprocessing, MCF was found to gain the ability to bind lipid PtdInsP5
342 and to undergo acetylation at the newly exposed N-terminal glycine. Recombinant MCF
343 stimulated to process *in vitro* was not blocked to Edman degradation, even using crude eukaryotic
344 cell lysate as a source of the host factor (Agarwal, Agarwal, et al., 2015). This observation
345 suggests that MCF could be acetylated only in vivo by host N-acetyltransferases when MCF is
346 present within cells Indeed, the ARF related protein ARFRP1 is N-terminal acetylated by NatC for
347 recruitment to the Golgi. In our case, we surmise the acetylation may aid retention of MCF at the
348 membrane following initial recruitment by ARFs. This retention may be augmented also by binding
349 to PtdInsP5.

350 Our electron microscopy and immunofluorescence studies reveal that expression of active
351 MCF in cells results in dramatic destruction of the Golgi and vesiculation of the cells. The
352 destruction of the Golgi occurred also during natural delivery of the effector from bacteria. Unlike
353 traditional IF techniques, using the novel cryoAPEX approach, the localization of MCF in cells
354 could be successfully visualized. Although possible that acetylation and binding PtdInsP5 initially
355 enriched MCF at the Golgi, the overexpressed protein is broadly distributed. It is found throughout

356 the cell, enriched also on mitochondrial membranes and possibly the nuclear membrane. This is
357 supported by cell fractionation that show MCF present in cytosol, nuclear, membrane, and
358 mitochondria fractions (Supplemental Fig 6). At late time points, there were many darkly stained
359 vesicles in the cell that might contain MCF although these are not easily distinguished by the
360 cryoAPEX method from dark staining lysosomes. The direct association with mitochondrial
361 membranes could explain the loss of the mitochondrial membrane potential that ultimately leads
362 to mitochondrial mediated apoptosis through activation of Caspases. Likewise, Golgi dispersion
363 is also known to induce apoptosis (Machamer, 2015). Thus, we identify the linkage of MCF to
364 ARFs as the likely cellular process that results in MCF mediated cell death, while the precise
365 molecular events subsequent to ARF stimulated activation of MCF remain to be resolved.

366 Other bacterial effectors have been identified as directly interacting with ARFs. For
367 example, *Shigella flexneri* Type III secretion effector IpaJ is a member of the C58 family of
368 cysteine peptidases but unlike MCF its activity depends on the canonical CHD active site.
369 Furthermore, IpaJ does not autoprocess but instead, it directly recognizes and cleaves the
370 myristoylated glycine of the lipid modified N-terminus of ARF1 and ARL GTPases. Similar to MCF,
371 IpaJ preferentially targets the GTP-bound active form of ARF1. By cleaving ARF1, IpaJ releases
372 the GTPase from the membrane, thus inducing Golgi disruption (Burnaevskiy et al., 2013).
373 However, despite extensive effort, our negative data support that MCF does not likewise directly
374 cause any processing or modification to ARFs as its mechanism for Golgi dispersion.

375 As noted above, ARFs are also allosteric activators of the ADP-ribosylating activity of
376 cholera toxin and related heat-labile toxins from enterotoxigenic *Escherichia coli* (Moss &
377 Vaughan, 1991). Similar to findings here, the N-terminal first 17 aa of ARF1 was dispensable for
378 activation of cholera toxin (Hong, Haun, Tsai, Moss, & Vaughan, 1994). The structure of cholera
379 toxin bound to ARF6 ultimately revealed that binding of ARF6 via its Switch 1 and Switch 2 regions
380 to face of CTA1 ~15 Å away from the CTA1 active site. Binding of ARF6 caused a structural
381 remodeling of the CTA1 loop regions to allow nicotinamide adenine dinucleotide to bind to the

382 active site for use to ADP-ribosylate the alpha subunit of the stimulatory G protein G_s (O'Neal,
383 Jobling, Holmes, & Hol, 2005). Thus, there is precedence in *Vibrios* for binding of ARFs as an
384 activator to stimulate structural remodeling of a bacterial effector, then without ARF for the effector
385 to function on a different target protein. Similar structural studies of MCF and MCF bound to ARFs
386 could elucidate these mechanisms for MCF.

387 These similarities support that stimulation by ARFs is a unifying theme for *Vibrio* toxins.
388 Although most *V. vulnificus* MARTX toxins have MCF, the MARTX toxin for Biotype 3 strains lack
389 this effector (Ziolo et al., 2014). However, these toxins do delivery a distinct MARTX effector we
390 designated DomainX (DmX). DmX is similar in size to MCF and likewise shows homology to the
391 C58 cysteine peptidases. However, DmX is only 22% identical to MCF and lacks the signature
392 RCD/Y motif. Further, the aligned His and Asp catalytic residues shared with the C58 peptidases
393 were found to be essential for DmX, whereas they were dispensable in MCF (Agarwal, Agarwal,
394 et al., 2015; Kim & Satchell, 2016). DmX was likewise found to autoprocess upon stimulation by
395 ARF1, ARF3, and ARF4; however, all three ARFs bound consistently with DmX in cells, unlike
396 MCF which shows a preference for ARF1. Expression of DmX in cells likewise results in
397 dispersion of the Golgi (Kim & Satchell, 2016). However, unlike MCF, DmX does not have an N-
398 terminus blocked to Edman degradation and is not thought to be post-translationally modified in
399 cells. In addition, catalytically inactive DmX is cytotoxic when expressed in cells, suggesting ARF
400 sequestering may play a more significant role in its cytotoxic mechanism. We postulate that these
401 two MARTX effectors have an evolutionarily shared mechanism for stimulated autoprocessing to
402 cause Golgi dispersion, but these two effectors have diverged to target the Golgi by distinct
403 molecular mechanism. Still, the presence of either MCF or DmX in nearly all *V. vulnificus* MARTX
404 toxins reveals that dissolution of vesicular trafficking is important for *V. vulnificus* pathogenesis.
405

406 **4. Materials and Methods**

407 **4.1 Tissue Culture**

408 Cos7 and HEK293T (generously provided by Dr. Richard Longnecker at Northwestern) cells were
409 prepared and cultured in Dulbecco's modified Eagle's medium (DMEM) supplemented with 10%
410 heat-inactivated fetal bovine serum (FBS) and 1% penicillin-streptomycin at 37°C in 5% CO_2.
411 Cells were seeded in 150 mm tissue culture dishes or 12-well tissue culture plates, and grown to
412 60 - 70% confluence.
413

414 **4.2 Bacterial strains and plasmids**

415 gBlocks containing Δ17 ARF1, Δ17 ARF3, Δ17 ARF4, Δ17 ARF6, ARF1, ARF3, MCF, MCF^{C148A},
416 cMCF, and $cMCF^{C148A}$ were synthesized by Integrated DNA Technologies (IDT) (Supplemental
417 Table 1). These fragments were cloned into SspI digested vector pMCSG7 using Gibson
418 assembly (New England Biolabs E2611L) (Antic, Biancucci, Zhu, Gius, & Satchell, 2015).
419 FLAG-MCF^{C148A}-HA, FLAG-$cMCF^{C148A}$-HA, FLAG-MCF-HA, FLAG-cMCF-HA, and MCF-eGFP
420 plasmids were generated as described in Agarwal *et al.* 2015.
421 ARF-Myc isoforms were constructed as in Kim and Satchell 2016. CMCP6 *rtxA1::bla* and
422 CMCP6 *rtxA1::mcf-bla V. vulnificus* strains were generated as detailed in Agarwal *et al.* 2015.
423 MCF-Apex2 was made by Gibson assembly using an APEX2 gBlock synthesized by IDT
424 (Supplemental Table 1) cloned into the FLAG-MCF-HA expression plasmid. GST-Δ17 ARF1 was
425 generously provided by Dr. Heike Folsch as described in Shteyn *et al.* 2011.
426

427 **4.3 Transfections and Western blotting**

428 For ectopic gene expression, cells were transfected using 1:3 μg of plasmid DNA to μl of 1 mg/mL
429 polyethylenimine. After 4 hours, the media was exchanged with fresh media. Following an
430 additional 14 hours, the cells were washed with phosphate buffered saline (PBS) and collected.
431 Whole cells were lysed in lysis buffer (300 mM NaCl, 20 mM Tris-HCl pH 8, 1.1% Triton X-100)
432 supplemented with ethylenediaminetetraacetic acid (EDTA) free protease inhibitor tablets

433 (Thermo Scientific A32965) incubated for an hour at 4°C and centrifuged to remove cell debris.
434 40 μg of total cell lysate was boiled for five minutes in 2× Laemmli sample buffer and separated
435 by SDS-PAGE, followed by transfer to nitrocellulose membrane with the BioRad Mini TransBlot
436 System. Western blots were then completed using anti-hemagglutinin (HA) (Sigma H6908), anti-
437 Myc (Thermo Scientific PA1-981), anti-MCF (produced with purified MCF protein by Lampire
438 Biological Laboratories, Pipersville PA), anti-ARF1 (Novus Biologicals NBP1-97935), anti-FLAG
439 (Sigma F3165), anti-mouse Immunoglobulin G (IgG) (Li-Cor 926-32210 or 926-68070), or
440 anti-rabbit IgG (Li-Cor 926-32211 or 926-68071) antibodies and visualized using the Li-Cor
441 Odyssey Fc imaging system.
442
443 **4.4 Immunoprecipitation**
444 Whole cell lysate was incubated overnight at 4°C with mouse IgG agarose (Sigma A0919),
445 agarose removed by centrifugation, and lysate subsequently incubated overnight with EZview™
446 Red Anti-c-Myc Affinity Gel or EZview™ Red Anti-HA Affinity Gel (Sigma E6779 and E6654).
447 Beads were washed with lysis buffer supplemented with EDTA-free protease inhibitor tablets four
448 times, once with 10 mM Tris-HCl pH 8.0, and protein eluted with 2 M NaSCN in 50 mM Tris-HCl
449 pH 8.0, 150 mM NaCl.
450
451 **4.5 Protein production and *in vitro* cleavage assays**
452 Plasmids were expressed in BL21 (DE3) *E. coli* (Wu, Christendat, Dharamsi, & Pai, 2000) to an
453 OD_{600} of 0.8 in terrific broth, induced with 1 M isopropyl β-D-1-thiogalactopyranoside and grown
454 overnight at 28°C. Cells were pelleted, lysed with a sonicator in Buffer A (10 mM Tris-HCl pH 8.0,
455 500 mM NaCl) with lysozyme, and cell debris removed by centrifugation. Δ17 ARF6 was
456 recovered from the insoluble fraction by incubation for one hour in Buffer A with 6 M Urea, followed
457 by centrifugation. Protein was then purified using the AKTA protein purification system with a Ni-

458 NTA HisTrap affinity column (GE Healthcare GE17-5248-02), followed by passage through a
459 Superdex 75 column for size exclusion chromatography. GST-Δ17 ARF1 was grown and lysate
460 collected as above and batch purified using glutathione sepharose (GE 17-0756-01).

461 Purified proteins were used for cleavage assays in which 2.5 μM of specified MCF and
462 4 μM ARF isoform were incubated in RAX buffer (20 mM Tris pH 7.5, 150 mM NaCl, 10 mM
463 $MgCl_2$) for various time points at 37°C, Laemmli sample buffer added, and boiled for five minutes
464 prior to separation by SDS-PAGE.

465

466 **4.6 Bacterial intoxication**

467 For bacterial treatments, mid-log phase CMCP6 *rtxA1::bla* and CMCP6 *rtxA1::mcf-bla*
468 *V. vulnificus* strains were pelleted and resuspended in PBS. Cos7 cells were washed twice with
469 PBS, treated with CMCP6 *rtxA1::bla* or CMCP6 *rtxA1::mcf-bla* at a MOI of 5 in DMEM, centrifuged
470 at 500 × *g* for three minutes, and incubated for an hour at 37°C with 5% CO_2.

471

472 **4.7 Fluorescence Microscopy**

473 For immunofluorescence microscopy, images were taken at the Northwestern University Center
474 for Advanced Microscopy using the Nikon A1R+ GaAsP Confocal Laser Microscope or the Nikon
475 N-SIM Structured Illumination Super-resolution Microscope.

476 Following treatment, cells grown on glass coverslips were washed with PBS and fixed with
477 4% formaldehyde for five minutes and permeabilized with 0.2% Tween 20. Cells were then
478 blocked with 10% goat serum in staining buffer (1% bovine serum albumin (BSA) plus 0.05%
479 Tween 20 in PBS) for one hour prior to staining with mouse anti-GM130 (BD Transduction
480 Laboratories 610822) or mouse anti-Calreticulin (abcam ab22683) diluted 1:200 in staining buffer
481 overnight. The coverslips were then washed five times for five minutes each time with staining
482 buffer. Secondary goat anti-mouse Alexa Fluor 647 antibody (Thermo Scientific) was then added

483 at 1:400 in staining buffer and incubated for one hour. The slides were washed twice with PBS
484 and twice with double distilled water with two minutes between each wash. The slides were
485 mounted using ProLong diamond antifade mountant with DAPI (4′,6′-diamidino-2-phenylindole)
486 (Invitrogen P36962).

487 For live cell imaging, cells were grown on 35/10 mm glass bottom tissue culture dishes
488 (Greiner Bio-One 627870). Prior to bacterial intoxication, cells were washed with PBS and
489 incubated with 150 nM MitoTracker™ Green FM (Thermo Fisher M7514) in DMEM for 45 minutes.
490 The cells were then washed with PBS and incubated with 5 μg/mL Hoescht 33342
491 (Immunochemistry Technologies 639) in PBS. After 10 minutes the cells were washed, fresh
492 DMEM added, and treated with bacteria as previously described. Images were taken every 5
493 minutes following intoxication for an hour.

494

495 **4.8 Electron microscopy and CryoAPEX localization**

496 HeLa cells were grown in 10 cm dishes and transfected with MCF-Apex2 using Lipofectamine
497 3000 (Thermo Fisher). Cells were trypsinized 10 or 15 hours post-transfection, resuspended in
498 DMEM and then pelleted at 500 x g. For live HPF cells were centrifuged and resuspended in 20%
499 BSA in PBS. Cells were pelleted and loaded onto copper membrane carriers (1mm x 0.5 mm;
500 Ted Pella Inc.) and cryofixed using the EM PACT2 high pressure freezer (Leica). Cryofixed cells
501 were processed by FS using an AFS2 automated FS unit (Leica) using the extended FS protocol
502 as described in Sengupta *et al*. 2019. For preparation of samples for cryoAPEX localization, cells
503 were instead resuspended in 0.1% sodium cacodylate buffer containing 2% glutaraldehyde for 30
504 minutes following trypsinization, washed three times with 0.1% sodium cacodylate buffer and
505 once with cacodylate buffer containing 1mg/ml 3,3'- DAB (Sigma-Aldrich). Pellets were then
506 incubated 20 minutes in 1mg/ml DAB (Sigma) and 5.88mM hydrogen peroxide (EM sciences) in
507 cacodylate buffer, pelleted and washed twice for 5 minutes in cacodylate buffer, once with DMEM,
508 once with DMEM 20% BSA, and pelleted again. These cells were loaded onto copper membrane

509 carriers and cryofixed as described before. An extended FS protocol was optimized for the
510 preferential osmication of the peroxidase-DAB byproduct to ascertain membrane association of
511 MCF. Briefly, frozen pellets were incubated for 60 hours at 90°C in acetone containing 5% water
512 and 1% osmium tetroxide then at -20°C for a 6 hour osmication cycle. For FS of direct HPF
513 samples, pellets were incubated for 24 hours at -90°C in acetone containing 0.2% tannic acid,
514 washed three times for 5 minutes with glass distilled acetone (EM Sciences), and resuspended
515 in acetone containing 5% water, 1% osmium tetroxide (OS) and 2% uranyl acetate (UA). Resin
516 exchange was carried out by infiltrating the sample with a gradually increasing concentration of
517 Durcupan ACM resin (Sigma-Aldrich) as follows: 2%, 4% and 8% for 2 hours each and then 15%,
518 30%, 60%, 90%, 100% and 100% + component C for 4 hours each. Samples were then
519 embedded in resin blocks and polymerized at 60°C for 36 hours. Post-hardening, planchets were
520 extracted by dabbing liquid nitrogen on the membrane carriers. Blocks were embedded a second
521 time and hardened at 60°C for 36 hours. Serial sections, 90 nm thick were obtained using a Leica
522 UC7 microtome. Serial-section ribbons were collected on formvar coated copper slot grids (EM
523 sciences). Sample grids from HPF processing were stained for an hour with 4% UA solution in
524 water followed by Sato's Lead. CryoAPEX samples were not post stained. Screening was carried
525 out using Tecnai-T12 transmission electron microscope operating at 80kV and images collected
526 with a Gatan 4K camera.
527
528 **4.9 Lipid overlay assays**
529 PIP Strip™ Membranes (Thermo Fisher P23750) were probed as per the manufacturer
530 instructions. Briefly, the membrane was blocked for an hour using TBS-T (10 mM Tris-HCl, pH
531 8.0, 150 mM NaCl, 0.1% Tween-20) + 3% fatty acid-free BSA (Sigma 126609) (TBS-T + BSA) for
532 an hour at room temperature. The His-tag was removed from purified MCF and cMCF proteins
533 using Tobacco Etch Virus (TEV) protease. Membranes were subsequently incubated with 0.5

534 μg/mL of either of these proteins in TBS-T + BSA overnight at 4°C and washed 10 times with
535 TBS-T + BSA. The membrane was then reprobed and washed as before. Bound protein was
536 detected using anti-MCF and anti-rabbit IgG antibodies as per the western blotting protocol.
537
538 **4.10 Two Dimensional Western analysis**
539 Anti-HA pulldowns of FLAG-MCF^{C148A}-HA, FLAG-cMCF^{C148A}-HA, FLAG-MCF-HA, and FLAG-
540 cMCF-HA recovered as described above were prepped using the Bio-Rad ReadyPrep 2-D
541 Cleanup Kit (Bio-Rad 1632130). The sample was then loaded onto 11 cm pH 3-10 immobilized
542 pH gradient (IPG) strips (Bio-Rad 1632014) and rehydrated overnight. Isoelectric focusing was
543 run on a Bio-Rad Protean IEF cell as per the Bio-Rad recommendations. Following IEF, the IPG
544 strip was equilibrated and analyzed by SDS-PAGE and western blotting.
545
546 **4.11 Mass Spectrometry Analysis**
547 Protein embedded in gel bands was digested with 200 ng trypsin (Thermo Scientific) at 37°C
548 overnight. Digest products were extracted from the gel bands in 50% acetonitrile/49.9%
549 water/0.1% trifluoroacetic acid (TFA) and desalted with C18 StageTips prior to analysis by tandem
550 mass spectrometry. Peptides were separated on an EASY-Spray HPLC column (25 cm × 75 μm
551 ID, PepMap RSLC C18, 2 μm, Thermo Scientific) using a gradient of 5 - 35% acetonitrile in 0.1%
552 formic acid and a flow rate of 300 nL/min for 45 minutes delivered by an EASY-nLC 1000 nUPLC
553 (Thermo Scientific). Tandem mass spectra were acquired in a data-dependent manner with an
554 Orbitrap Q Exactive mass spectrometer (Thermo Fisher Scientific) interfaced to a
555 nanoelectrospray ionization source.
556 The raw MS/MS data were converted into MGF format by Thermo Proteome Discoverer
557 (VER. 1.4, Thermo Scientific). The MGF files were then analyzed by a MASCOT sequence
558 database search. The search was performed using fixed modifications of Met oxidation and Cys

559 carbamidomethylation and variable modifications of Lys acetylation and N-terminal acetylation.
560 Mass accuracy of 10 ppm on precursor ions and 15 ppm of fragment ions were allotted. Peptides
561 identified by the MASCOT search were then manually validated.

562 To determine the activator of MCF, pulldowns completed on FLAG-cMCF^{C148A}-HA,
563 ectopically expressed in HEK293T cells were analyzed for total protein identification by mass
564 spectrometry at the University of Illinois at Chicago Mass Spectrometry Core.

565

566 **ACKNOWLEDGEMENTS**

567 The authors thank Heike Folsch for sharing ARF expression plasmids. We thank the Purdue
568 CryoEM Facility at Hockmeyer Hall for access to the high-pressure freezer, freeze substitution
569 unit, microtome and chemical hood. We thank Dr. Christopher Gilpin for access to the T12
570 electron microscope at the Purdue Life Sciences EM Core Facility where thin sectioning was
571 carried out. We also thank Dr. Arvanitis and the Center for Advanced Microscopy and Nikon
572 Imaging Center at Northwestern University for their invaluable help and resources. This work was
573 supported by National Institutes of Health grants AI092825 (to K.J.F.S), R01GM10092 (to S.M.),
574 as well as Indiana Clinical and Translational Sciences Institute grant CTSI-106564 (to S.M.), and
575 Purdue University Institute for Inflammation, Immunology and Infectious Diseases grant PI4D-
576 209263 (to S.M.), GM104610 (to R.R.O.L.), and GM103479 (to J.A.L.). A.H. was supported by a
577 Ruth L. Kirschstein Institutional National Research Service Award (5T32AI007476). J.M. was
578 supported by a UCLA Molecular Biology Institute Whitcome Fellowship. Immunoflourescence
579 imaging work was performed at the Northwestern University Center for Advanced Microscopy
580 generously supported by NCI CCSG P30 CA060553 awarded to the Robert H Lurie
581 Comprehensive Cancer Center.

582

583 **CONFLICTS OF INTEREST**

584 The authors declare no conflicts of interest

585 **ORCID**

586 Alfa Herrera / https://orcid.org/0000-0002-7081-4208

587 Rachel R Ogorzalek Loo / https://orcid.org/0000-0002-0580-2833

588 Joseph A Loo / https://orcid.org/0000-0001-9989-1437

589 Seema Mattoo / https://orcid.org/0000-0003-3260-0046

590 Karla J F Satchell / https://orcid.org/0000-0003-3274-7611
591

592 **REFERENCES**

593 Agarwal, S., Agarwal, S., Biancucci, M., & Satchell, K. J. (2015). Induced autoprocessing of the
594 cytopathic Makes caterpillars floppy-like effector domain of the Vibrio vulnificus MARTX toxin.
595 *Cell Microbiol, 17*(10), 1494-1509. doi:10.1111/cmi.12451

596 Agarwal, S., Zhu, Y., Gius, D. R., & Satchell, K. J. (2015). The Makes Caterpillars Floppy (MCF)-Like
597 Domain of Vibrio vulnificus Induces Mitochondrion-Mediated Apoptosis. *Infect Immun, 83*(11),
598 4392-4403. doi:10.1128/IAI.00570-15

599 Antic, I., Biancucci, M., Zhu, Y., Gius, D. R., & Satchell, K. J. F. (2015). Site-specific processing of Ras
600 and Rap1 Switch I by a MARTX toxin effector domain. *Nat Commun, 6*, 7396.
601 doi:10.1038/ncomms8396

602 Backer, J. M. (2010). New methods for capturing the mystery lipid, PtdIns5P. *Biochem J, 428*(3), e1-2.
603 doi:10.1042/BJ20100688

604 Baker-Austin, C., Trinanes, J. A., Taylor, N. G. H., Hartnell, R., Siitonen, A., & Martinez-Urtaza, J. (2012).
605 Emerging Vibrio risk at high latitudes in response to ocean warming. *Nature Climate Change,*
606 *3*(1), 73-77. doi:10.1038/nclimate1628

607 Behnia, R., Panic, B., Whyte, J. R., & Munro, S. (2004). Targeting of the Arf-like GTPase Arl3p to the
608 Golgi requires N-terminal acetylation and the membrane protein Sys1p. *Nat Cell Biol, 6*(5), 405-
609 413. doi:10.1038/ncb1120

610 Burnaevskiy, N., Fox, T. G., Plymire, D. A., Ertelt, J. M., Weigele, B. A., Selyunin, A. S., . . . Alto, N. M.
611 (2013). Proteolytic elimination of N-myristoyl modifications by the Shigella virulence factor IpaJ.
612 *Nature, 496*(7443), 106-109. doi:10.1038/nature12004

613 CDC. (2014). Cholera and Other Vibrio Illness Surveillance (COVIS) Annual summaries 2008-2014.
614 Retrieved from http://www.cdc.gov/nationalsurveillance/cholera-vibrio-surveillance.html
615 Deeb, R., Tufford, D., Scott, G. I., Moore, J. G., & Dow, K. (2018). Impact of Climate Change on Vibrio
616 vulnificus Abundance and Exposure Risk. *Estuaries Coast, 41*(8), 2289-2303.
617 doi:10.1007/s12237-018-0424-5
618 Gavin, H. E., & Satchell, K. J. (2015). MARTX toxins as effector delivery platforms. *Pathog Dis, 73*(9),
619 ftv092. doi:10.1093/femspd/ftv092
620 Gillingham, A. K., & Munro, S. (2007). The small G proteins of the Arf family and their regulators. *Annu*
621 *Rev Cell Dev Biol, 23*, 579-611. doi:10.1146/annurev.cellbio.23.090506.123209
622 Gulig, P. A., Bourdage, K. L., & Starks, A. M. (2005). Molecular Pathogenesis of Vibrio vulnificus. *J*
623 *Microbiol, 43 Spec No*, 118-131.
624 Hoffman, S. M., Bryan;, & Batz, M. (2015). Economic Burden of Major Foodborne Illnesses Acquired in
625 the United States. *United States Department of Agriculture, Economic Research Service*.
626 Hofmann, I., & Munro, S. (2006). An N-terminally acetylated Arf-like GTPase is localised to lysosomes
627 and affects their motility. *J Cell Sci, 119*(Pt 8), 1494-1503. doi:10.1242/jcs.02958
628 Hong, J. X., Haun, R. S., Tsai, S. C., Moss, J., & Vaughan, M. (1994). Effect of ADP-ribosylation factor
629 amino-terminal deletions on its GTP-dependent stimulation of cholera toxin activity. *J Biol Chem,*
630 *269*(13), 9743-9745.
631 Horseman, M. A., & Surani, S. (2011). A comprehensive review of Vibrio vulnificus: an important cause of
632 severe sepsis and skin and soft-tissue infection. *Int J Infect Dis, 15*(3), e157-166.
633 doi:10.1016/j.ijid.2010.11.003
634 Kahn, R. A., Randazzo, P., Serafini, T., Weiss, O., Rulka, C., Clark, J., . . . Rothman, J. E. (1992). The
635 amino terminus of ADP-ribosylation factor (ARF) is a critical determinant of ARF activities and is a
636 potent and specific inhibitor of protein transport. *J Biol Chem, 267*(18), 13039-13046.
637 Kim, B. S. (2018). The Modes of Action of MARTX Toxin Effector Domains. *Toxins (Basel), 10*(12).
638 doi:10.3390/toxins10120507
639 Kim, B. S., & Satchell, K. J. (2016). MARTX effector cross kingdom activation by Golgi-associated ADP-
640 ribosylation factors. *Cell Microbiol, 18*(8), 1078-1093. doi:10.1111/cmi.12568

641 King, M., Rose, L., Fraimow, H., Nagori, M., Danish, M., & Doktor, K. (2019). Vibrio vulnificus Infections
642 From a Previously Nonendemic Area. *Ann Intern Med*. doi:10.7326/L19-0133
643 Kwak, J. S., Jeong, H. G., & Satchell, K. J. (2011). Vibrio vulnificus rtxA1 gene recombination generates
644 toxin variants with altered potency during intestinal infection. *Proc Natl Acad Sci U S A, 108*(4),
645 1645-1650. doi:10.1073/pnas.1014339108
646 Lee, B. C., Choi, S. H., & Kim, T. S. (2008). Vibrio vulnificus RTX toxin plays an important role in the
647 apoptotic death of human intestinal epithelial cells exposed to Vibrio vulnificus. *Microbes Infect,*
648 *10*(14-15), 1504-1513. doi:10.1016/j.micinf.2008.09.006
649 Liu, S., & Storrie, B. (2015). How Rab proteins determine Golgi structure. *Int Rev Cell Mol Biol, 315*, 1-22.
650 doi:10.1016/bs.ircmb.2014.12.002
651 Machamer, C. E. (2015). The Golgi complex in stress and death. *Front Neurosci, 9*, 421.
652 doi:10.3389/fnins.2015.00421
653 Mead, P. S., Slutsker, L., Dietz, V., McCaig, L. F., Bresee, J. S., Shapiro, C., . . . Tauxe, R. V. (1999).
654 Food-related illness and death in the United States. *Emerg Infect Dis, 5*(5), 607-625.
655 Morgan, K. L., Thomas J. Stevens III, and Robert L. Degner. (2010). Economic Impacts of Alternative
656 Regulatory Scenarios on the Florida Fresh Half Shell Oyster Industry.
657 Moss, J., & Vaughan, M. (1991). Activation of cholera toxin and Escherichia coli heat-labile enterotoxins
658 by ADP-ribosylation factors, a family of 20 kDa guanine nucleotide-binding proteins. *Mol*
659 *Microbiol, 5*(11), 2621-2627. doi:10.1111/j.1365-2958.1991.tb01971.x
660 Muthamilarasan, M., Mangu, V. R., Zandkarimi, H., Prasad, M., & Baisakh, N. (2016). Structure,
661 organization and evolution of ADP-ribosylation factors in rice and foxtail millet, and their
662 expression in rice. *Sci Rep, 6*, 24008. doi:10.1038/srep24008
663 O'Neal, C. J., Jobling, M. G., Holmes, R. K., & Hol, W. G. (2005). Structural basis for the activation of
664 cholera toxin by human ARF6-GTP. *Science, 309*(5737), 1093-1096.
665 doi:10.1126/science.1113398
666 Rawlings, N. D., Waller, M., Barrett, A. J., & Bateman, A. (2014). MEROPS: the database of proteolytic
667 enzymes, their substrates and inhibitors. *Nucleic Acids Res, 42*(Database issue), D503-509.
668 doi:10.1093/nar/gkt953

669 Roig, F. J., Gonzalez-Candelas, F., & Amaro, C. (2011). Domain organization and evolution of
670 multifunctional autoprocessing repeats-in-toxin (MARTX) toxin in Vibrio vulnificus. *Appl Environ*
671 *Microbiol, 77*(2), 657-668. doi:10.1128/AEM.01806-10
672 Satchell, K. J. F. (2015). Multifunctional-autoprocessing repeats-in-toxin (MARTX) Toxins of Vibrios.
673 *Microbiol Spectr, 3*(3). doi:10.1128/microbiolspec.VE-0002-2014
674 Sengupta, R., Poderycki, M. J., & Mattoo, S. (2019). CryoAPEX - an electron tomography tool for
675 subcellular localization of membrane proteins. *J Cell Sci, 132*(6). doi:10.1242/jcs.222315
676 Tsai, S. C., Adamik, R., Haun, R. S., Moss, J., & Vaughan, M. (1993). Effects of brefeldin A and
677 accessory proteins on association of ADP-ribosylation factors 1, 3, and 5 with Golgi. *J Biol Chem,*
678 *268*(15), 10820-10825.
679 Wei, J. H., & Seemann, J. (2010). Unraveling the Golgi ribbon. *Traffic, 11*(11), 1391-1400.
680 doi:10.1111/j.1600-0854.2010.01114.x
681 Wu, N., Christendat, D., Dharamsi, A., & Pai, E. F. (2000). Purification, crystallization and preliminary X-
682 ray study of orotidine 5'-monophosphate decarboxylase. *Acta Crystallogr D Biol Crystallogr, 56*(Pt
683 7), 912-914. doi:10.1107/s090744490000576x
684 Ziolo, K. J., Jeong, H. G., Kwak, J. S., Yang, S., Lavker, R. M., & Satchell, K. J. (2014). Vibrio vulnificus
685 biotype 3 multifunctional autoprocessing RTX toxin is an adenylate cyclase toxin essential for
686 virulence in mice. *Infect Immun, 82*(5), 2148-2157. doi:10.1128/IAI.00017-14

687 **SUPPORTING INFORMATION**

688 Additional supporting information for this file includes six supplemental figures and one
689 supplemental table.

690 **Supplemental Figure 1.** MCF does not cleave or directly modify ARF1 or ARF3.
691 A-G. Bottom-up mass spectrometry was performed on ARF1 and ARF3 samples recovered from
692 recombinant (A) (B) or anti-Myc IPs (C-G) from HEK293T cells transfected or incubated with and
693 without MCF or MCF^{CA}. Modifications that were detected are denoted. Any modifications found
694 on either ARF1 or ARF3 were not reproducible across replicates. Furthermore, There were no

695 modifications detected that were found in ARF + MCF samples that were not found in ARF
696 samples alone and thus not attributable to MCF.
697 **Supplemental Figure 2.** Edman degradation is blocked in MCF recovered from cells.
698 A. Reads from Edman degradation analysis completed on dt-MCF immunoprecipitated from
699 HEK293T cell lysate using anti-HA antibody. No signal and very little background was detected.
700 B. Gel of sample used for analysis.
701 **Supplemental Figure 3.** MCF is N-terminally acetylated inside host cells.
702 Replicates of two-dimensional gel analysis of dt-MCF expressed in HEK293T cells, recovered by
703 anti-HA immunoprecipitation. Amino acids acetylated in each circled population indicated in
704 corresponding color on sequence.
705 **Supplemental Figure 4.** MCF does not alter normal endoplasmic reticulum structure.
706 Cos7 cells were transfected with empty vector or MCF-EGFP (green) for 18 hours, fixed, and
707 stained for DAPI (blue), and endoplasmic reticulum marker (calreticulin) (red).
708 **Supplemental Figure 5.** Transmission electron microscopy shows Golgi vesiculation induced
709 by MCF.
710 A, B. Electron microscopy tomograms taken of HeLa cells ectopically expressing MCF for 10 (A)
711 or 15 hours (B). A-D. On right, higher magnification of boxed region on left showing Golgi (G),
712 herniated Golgi (red arrows), vesicles (V). and autolysomes (A).
713 **Supplemental Figure 6.** Western blot of subcellular fractions from HEK 293T cells ectopically
714 expressing dt-MCF. Each fraction probed with standards for membrane (CD-44), mitochondria
715 (Hsp-60), and nucleus (HistoneH3), and MCF (anti-HA).
716 **Supplemental Table 1.** Sequences of gBlocks used for plasmid construction
717

718

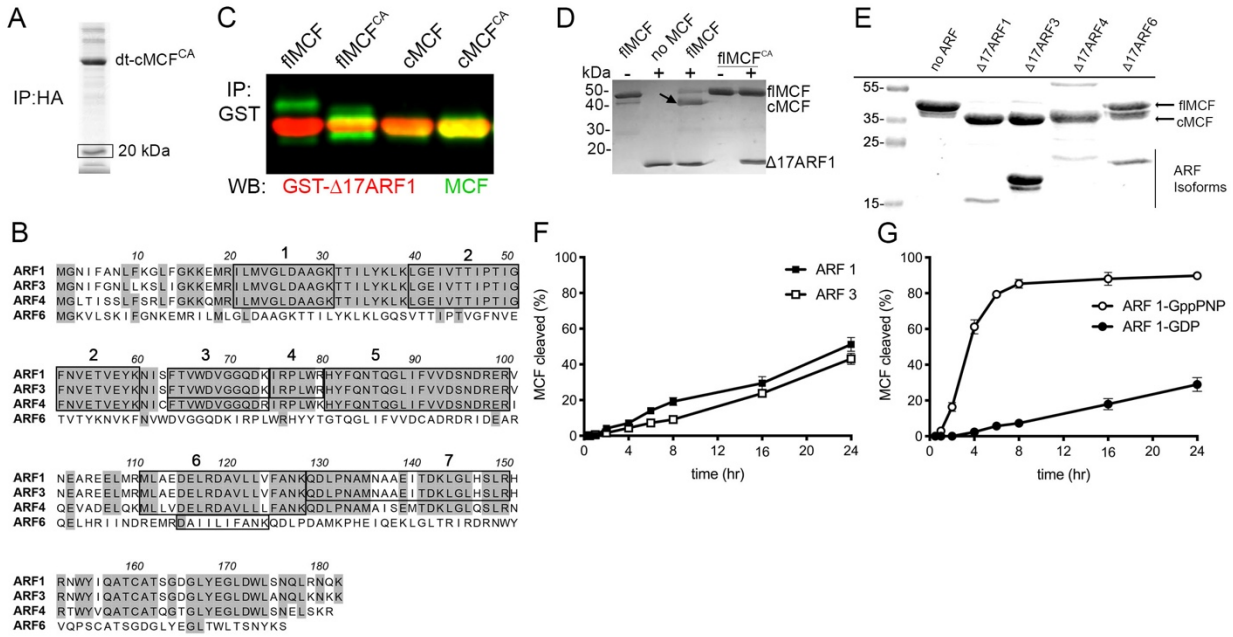

719

720 **Figure 1.** MCF autoproteolytic cleavage is induced by ARF GTPases.

721 A. dt-cMCF^{CA} was immunoprecipitated (IP) from HEK293T cell lysate using anti-HA antibody. Box
722 indicates band excised for mass spectrometry peptide sequencing. B. Amino acid sequence
723 alignment of major isoforms of ARFs with boxes indicating identified peptides. C. Purified
724 GST-Δ17 ARF1 was incubated with either MCF, MCF^{CA}, cMCF, or cMCF^{CA} at 37°C. Western blot
725 on samples following anti-GST IP using anti-MCF (green bands) and anti-ARF1 (red bands).
726 showing catalytically active and inactive flMCF and cMCF (green bands) can bind ARF1(red
727 bands) *in vitro*. D. Recombinant flMCF and flMCF^{CA} incubated with ΔARF1 indicate induced
728 autoprocessing is dependent on MCF catalytic active site. E. Auto-cleavage induced by purified
729 ARF isoforms incubated with MCF for 24 hours. F, G. Autoprocessing of flMCF at 37°C for time
730 indicated induced by full-length ARF1 or ARF3 (F) or with ARF1 pre-loaded with GDP or non-
731 hydrolyzable GTP (GppNHp) (G). Representative gels (n>3), with percent cleaved MCF was
732 determined by densitometry of bands on Coomassie stained gels (%=(cMCF/(cMCF+flMCF)*100
733 from three independent reactions.

734

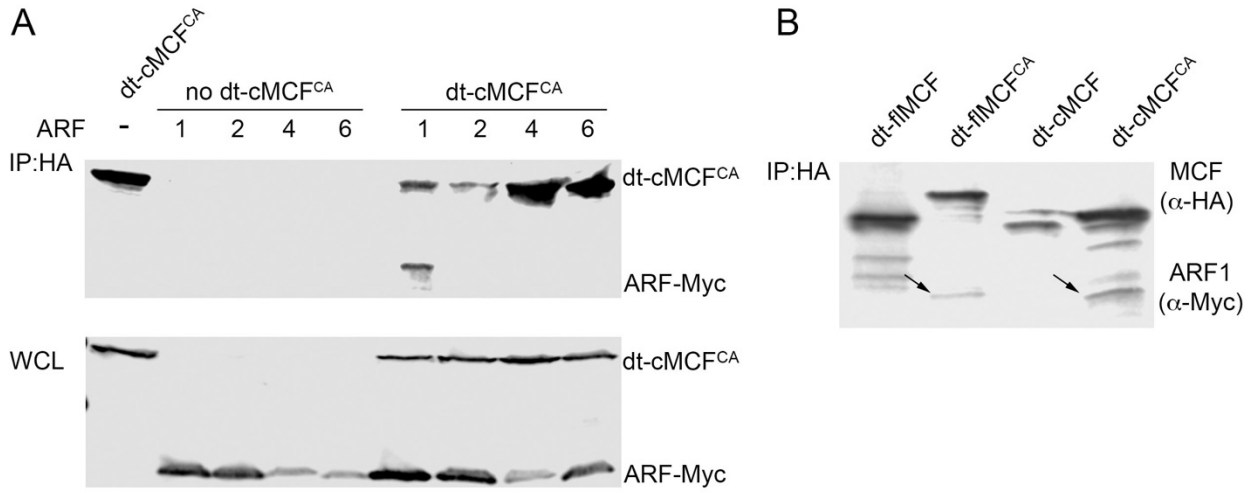

735

736 **Figure 2.** MCF^{CA} stably associates ARF1 in HEK293T cells.

737 A. HEK293T cells were co-transfected with dt-cMCF^{C148A} and either Myc-tagged ARF1, 3, 4, or 6.

738 Western blot of whole cell lysates (bottom) recovered from cells. Western blot after IP using anti-

739 HA beads (top). MCF and ARFs detected by anti-HA and anti-Myc antibodies respectively. B.

740 HEK293T cell were co-transfected with ARF1-Myc and either dt-flMCF, dt-flMCF^{CA}, dt-cMCF, or

741 dt-cMCF^{CA}. Western blot on cell lysates recovered from these cells following anti-HA IP as in (A).

742

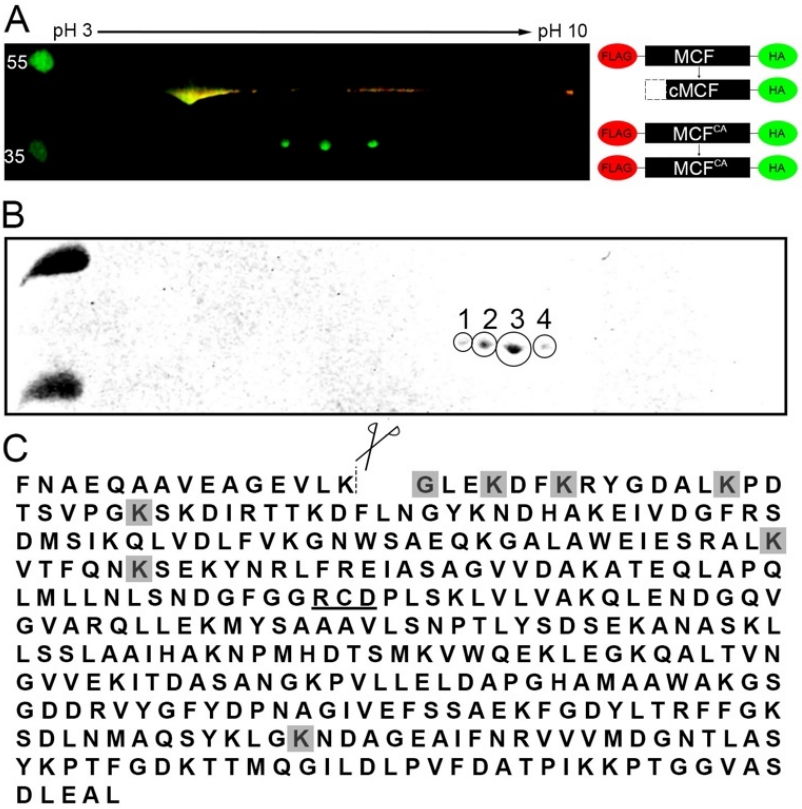

Figure 3. MCF is N-terminally acetylated following auto-cleavage.

A. Anti-HA IP on cell lysates of HEK293T cells ectopically expressing dt-MCF or dt-MCF^{CA} was individually completed. Samples were then combined for two-dimensional western analysis using IPG strips pH 3-10 with western blot completed using anti-FLAG (red) and anti-HA (green) antibodies. B. Two-dimensional analysis with Coomassie gel was completed using dt-MCF as in (A). Gel shows populations that were individually excised and analyzed by bottom up mass spectrometry. C. Protein sequence of MCF designating auto-cleavage site (dashed-line), and catalytic residues important for auto-proteolytic activity (underlined). Shaded residues are those found to be acetylated in populations 1-4.

Spot #	PIP Strips * and PIP MicroStrips †
1	Lysophosphatidic acid
2	Lysophosphatidylcholine
3	Phosphatidylinositol (PtdIns)
4	PtdIns(3)P
5	PtdIns(4)P
6	PtdIns(5)P
7	Phosphatidylethanolamine
8	Phosphatidylcholine
9	Sphingosine 1-phosphate
10	PtdIns(3,4)P_2
11	PtdIns(3,5)P_2
12	PtdIns(4,5)P_2
13	PtdIns(3,4,5)P_3
14	Phosphatidic acid
15	Phosphatidylserine
16	Blank

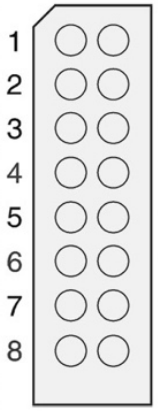

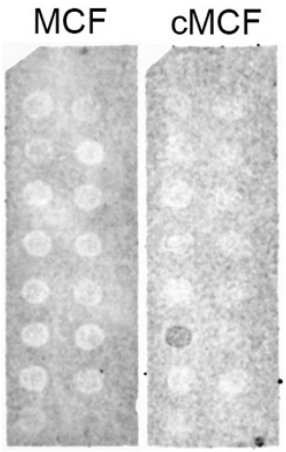

Figure 4. MCF associates with Golgi associated lipids.

Lipid overlay assay was conducted using PIP Strips™ with either purified flMCF or cMCF. Blot shows cMCF binds phosphatidylinositol-5-phosphate.

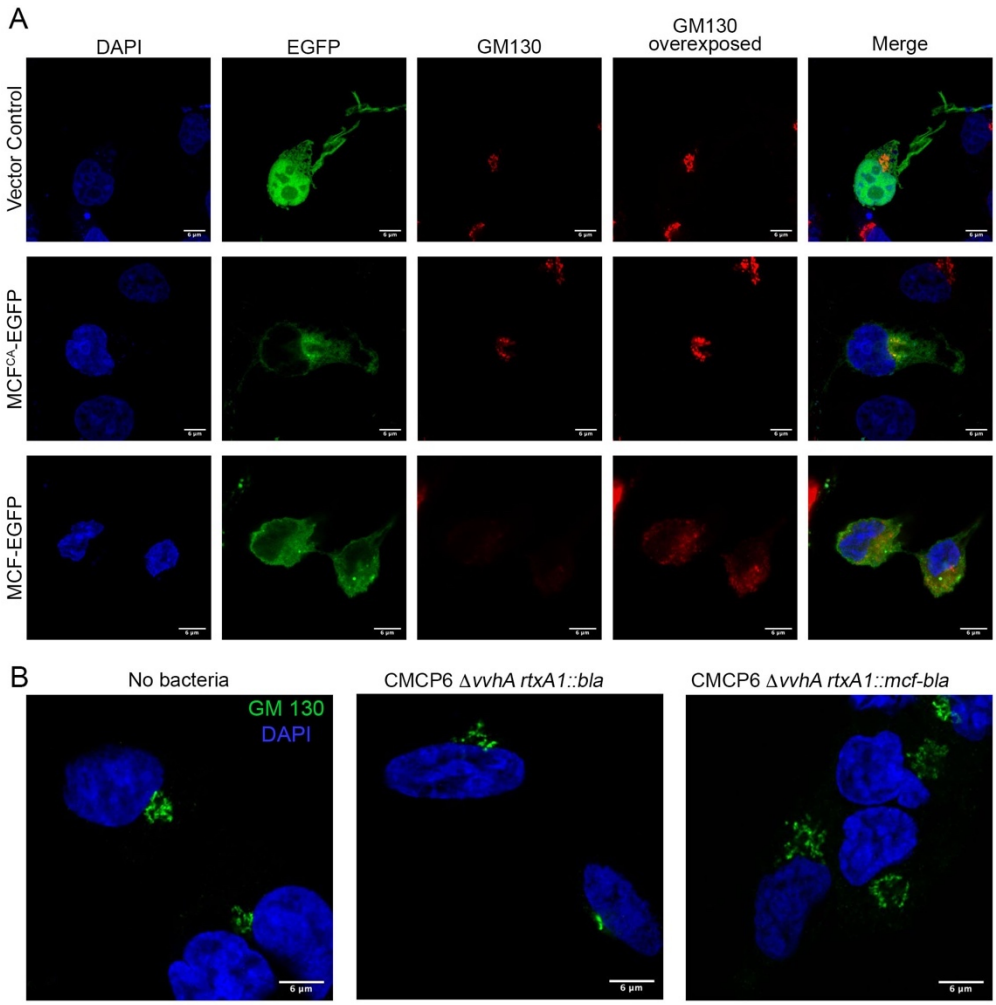

760

761 **Figure 5.** MCF induces Golgi dispersion.

762 A. Cos7 cells were transfected with empty vector, MCF^{CA}-EGFP, or MCF-EGFP (green) for 18

763 hours, fixed, and stained for DAPI (blue), and *cis*-Golgi marker (GM130) (red). B. Cos7 cells were

764 infected with CMCP6 *rtxA1::bla* or CMCP6 *rtxA1::mcf-bla* at a MOI of 5 for an hour, fixed, and

765 stained for DAPI (blue), and *cis*-Golgi marker (GM130) (green).

766

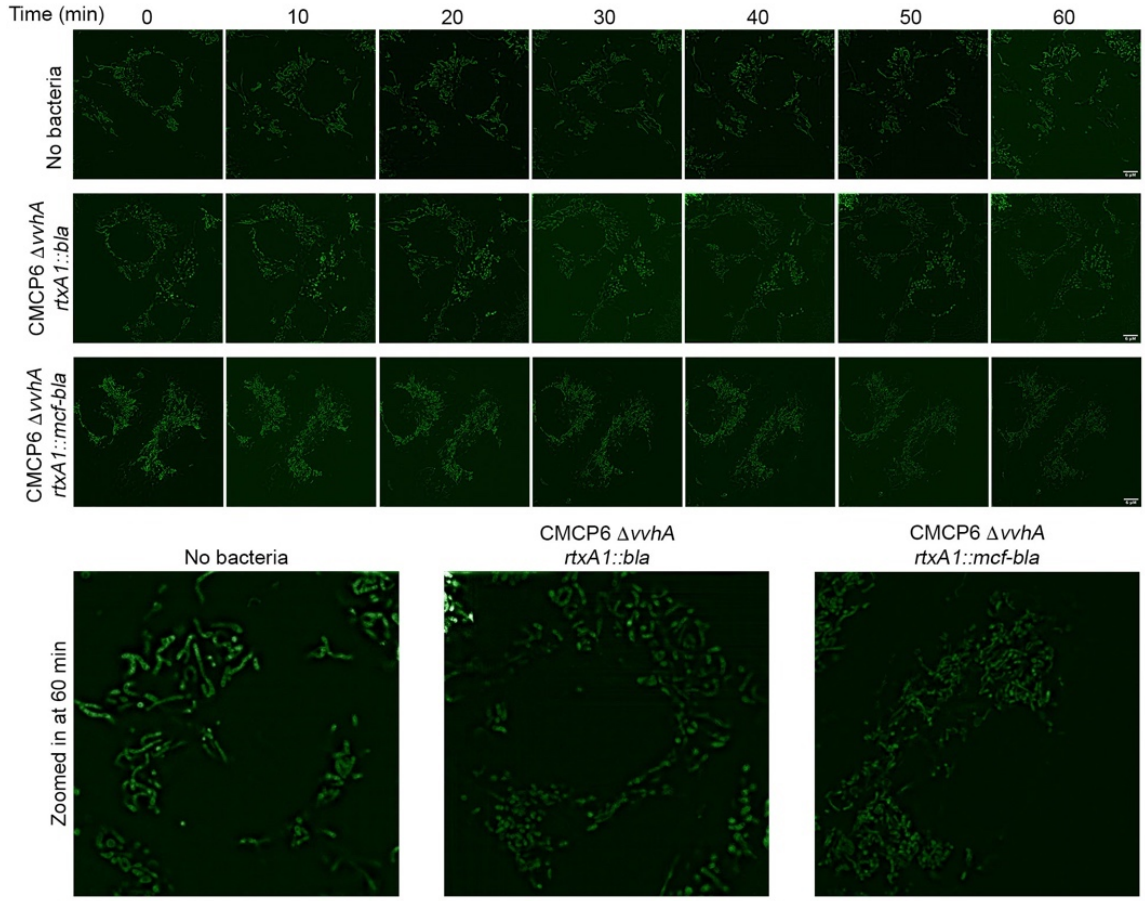

767

768 **Figure 6.** MCF disrupts the mitochondrial network.

769 A. Cos7 cells were incubated with MitoTracker™ Green FM to visualize mitochondria prior to

770 infection with CMCP6 *rtxA1::bla* or CMCP6 *rtxA1::mcf-bla* at a MOI of 5 for an hour. Images taken

771 prior to intoxication and every 10 minutes after. Insets show enlarged image of one cell for each

772 condition at 60 minutes.

773

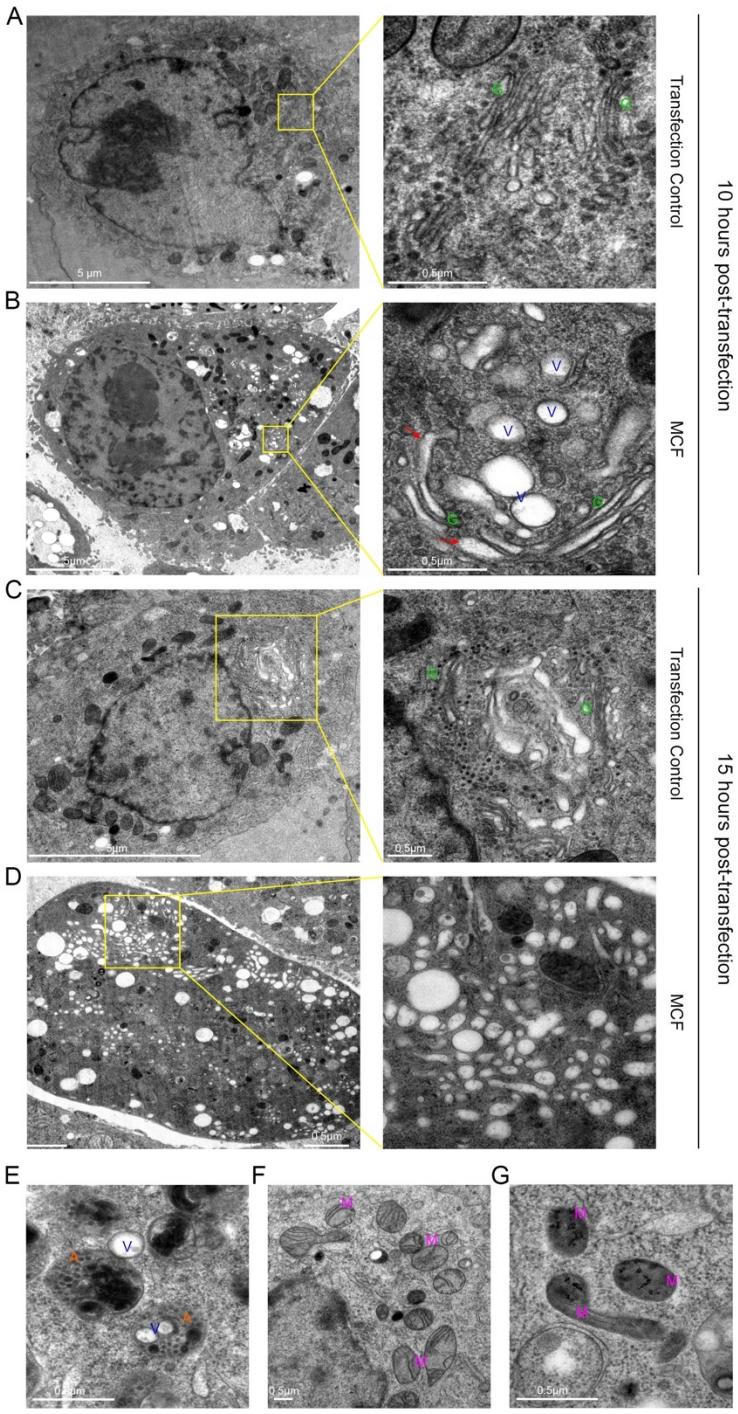

774

775 **Figure 7.** MCF causes vesiculation of the Golgi apparatus as seen by transmission electron

776 microscopy.

777 A-G. Thin-section electron microscopy of HeLa cells ectopically expressing MCF, or mock
778 transfected for either 10 (A)(B) or 15 hours (C)(D) post-transfection. A-D. On right, higher
779 magnification of boxed region on left showing Golgi (G), herniated Golgi (red arrows), and vesicles
780 (V). E. Autolysomes (A) clearing MCF induced vesicles. F, G. Mitochondria (M) of mock
781 transfected cells (F) and MCF transfected cells (G) at 10 hours post-transfection.
782

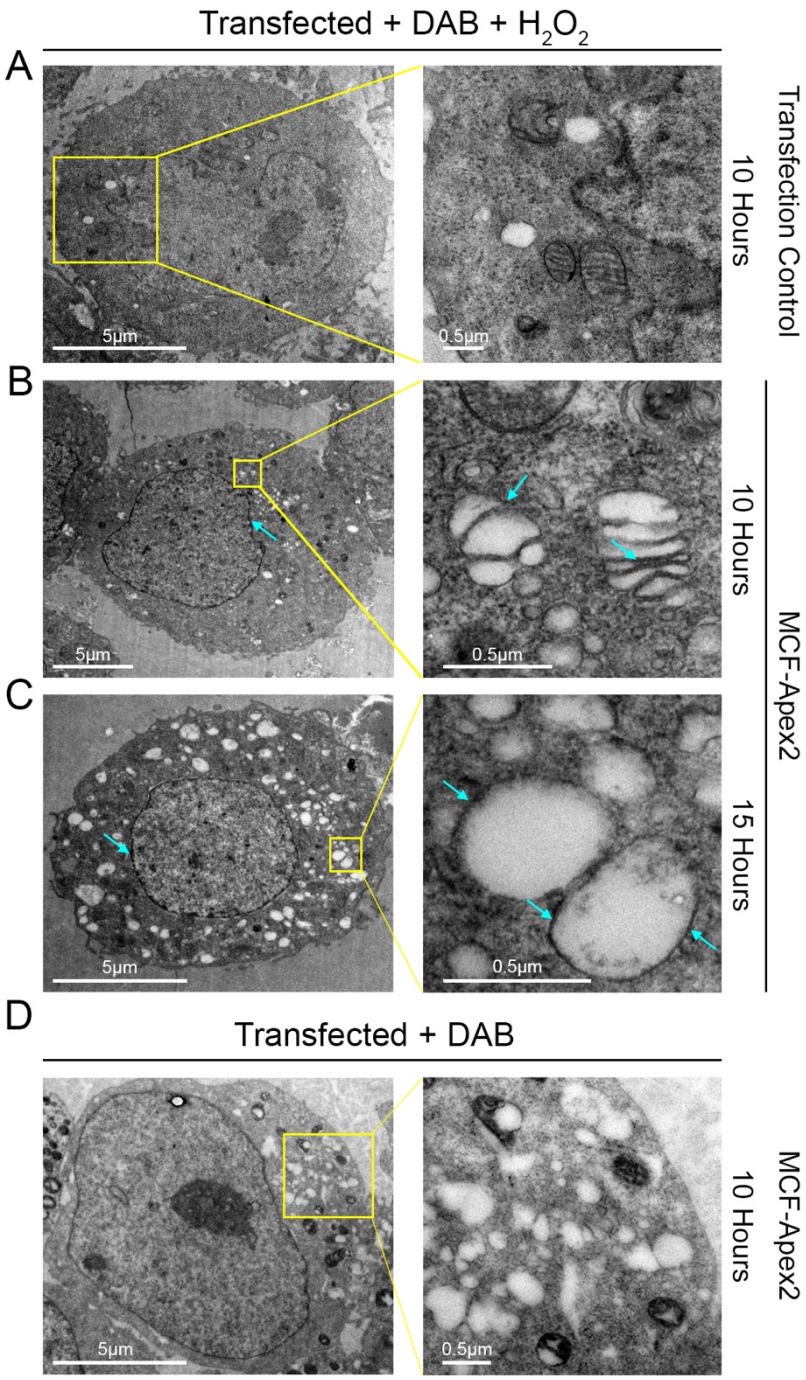

783

784 **Figure 8.** MCF concentrates in the cytoplasm, Golgi cisternae, and nuclear and vesicle

785 membranes.

786 A-D. Thin-section electron microscopy of resin embedded HeLa cells treated with

787 diaminobenzidine (DAB) + H_2O_2 (A-C) or just DAB (D) ectopically expressing MCF (B) (C) (D), or

788 mock transfected (A) for either 10 or 15 hours post-transfection. On right, higher magnification of
789 boxed region on left. B-D. Light blue arrows show darkened Apex 2 staining, indicating high
790 concentrations of MCF, seen with H_2O_2 treatment (B) (C) and not without (D).
791